Realization of a spin-incoherent Luttinger liquid

Danyel Cavazos-Cavazos,[1] Ruwan Senaratne,[1] Aashish Kafle,[1] and Randall G. Hulet[1,*]

[1] *Department of Physics and Astronomy, Rice University, Houston, Texas 77005, USA*

(Dated: October 13, 2022)

The Tomonaga-Luttinger liquid (TLL) theory describes the low-energy excitations of strongly correlated one-dimensional (1D) fermions. In the past years, a number of studies have provided a detailed understanding of this universality class. More recently, theoretical investigations that go beyond the standard low-temperature, linear-response, TLL regime have emerged as an active area of research. While these provide a basis for understanding the dynamics of the spin-incoherent Luttinger liquid, there are few experimental investigations in this regime. Here we report the observation of a thermally-induced spin-incoherent Luttinger liquid in an atomic Fermi gas confined to 1D. We use Bragg spectroscopy to measure the suppression of spin-charge separation and the decay of correlations as the temperature is increased. Our results probe the crossover between the coherent and incoherent regimes of the Luttinger liquid, and elucidate the interplay between the charge and the spin degrees of freedom in this regime.

Studies of strongly interacting atomic gases in 1D, aided by exactly solvable models[1–6], have provided remarkable insight into the physics of highly-correlated quantum many-body systems with regimes that are increasingly accessible to experiment[7–14]. The low-energy properties of fermions in 1D are particularly well understood in terms of the TLL theory [15–19], which exhibits a spin-charge separation of the low-energy collective spin- and charge-density waves (SDWs/CDWs) that are bosonic in nature and propagate with different velocities. At its core, the standard TLL universality class is characterized by collective excitations that are coherent and linearly dispersing. Several regimes, however, have been found to extend beyond this spin-charge separation paradigm, allowing access to new classes of unconventional Luttinger liquids where the coherence of the excitations is disrupted[20–22]. The introduction of higher-order interaction effects such as band-curvature and backscattering, for example, gives rise to the so-called nonlinear Luttinger liquid [23], for which the linearity of the dispersion is disrupted. Spin polarization is expected to control a quantum phase transition, at which the TLL turns quantum critical and all thermodynamic quantities exhibit universal scaling[22]. Allowing for anisotropic coupling between 1D chains of fermions could realize the sliding Luttinger liquid (SLL) phase[24]. Topological materials such as single- and bi-layer graphene [25] may enable access to phases such as chiral Luttinger liquids[26] (χLL), which host excitation modes with a preferred sense of propagation.

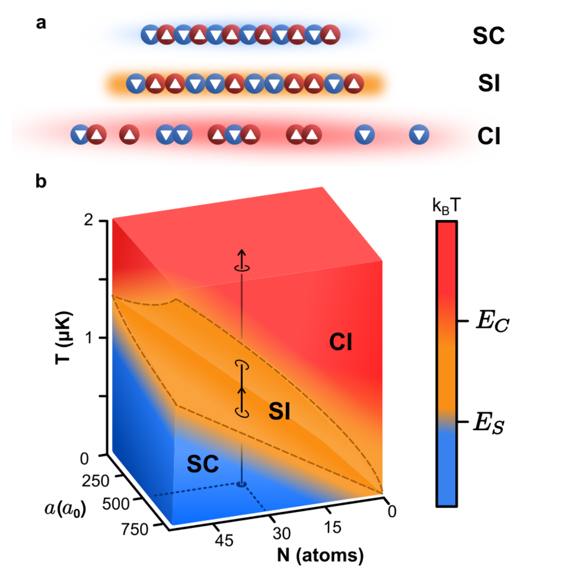

Fig. 1. Energy hierarchy of a Luttinger liquid. **a**, Schematic diagram showing the energy regimes of a Luttinger liquid in the spin-coherent (SC), spin-incoherent (SI) and charge-incoherent (CI) regimes, illustrating the effect of decoherence of the spin and charge correlations. **b**, Crossover hierarchy of a quasi-1D atomic Fermi gas (see Methods). The incoherent regimes can be reached either by increasing the scattering length a, increasing the temperature T, or by reducing the number of atoms per tube, N. Dashed lines correspond to the boundaries between the different regimes, defined by $E_s \simeq k_BT$ and $E_c \simeq k_BT$. Solid line illustrates a trajectory corresponding to constant N and a. As T is increased, the system first loses its spin coherence for $E_s < k_BT < E_c$, and at a sufficiently high T, such that $E_s < E_c < k_BT$, all coherence in the system is lost.

Finite temperature represents another pathway for disrupting the correlations in a TLL (Fig. 1a). In the low temperature (T) limit, the thermal energy k_BT is the lowest energy scale and both the charge- and spin-density waves propagate coherently in accordance with the standard TLL theory, thus defining the spin-coherent (SC) regime. As T is increased, thermal fluctuations disrupt the coherence in the spin sector first, and the system enters the spin-incoherent (SI) Luttinger liquid regime[27]. In the SI regime, spin-spin correlations are expected to exhibit a rapid exponential decay while the density-density correlations retain a slower algebraic decay, leading to correlations that are completely independent from the spin sector[28]. The SI regime has been investigated theoretically with the Bethe ansatz [28, 29] and a bosonized path integral approach [30–32] to describe both fermions[33] and bosons[34]. Recent studies have also identified density correlations [28, 33, 35] that distinguish the SC and the SI regimes. Experimental evidence for the SI regime, however, remains scarce. Studies of quasi-1D solid-state materials using angle-resolved photoemission spectroscopy [36, 37] have suggested that signatures of the SI arise for small electron densities[38]. The control and tunability afforded by ultracold gases, on the other hand, have proven to be advantageous for the systematic study of Luttinger liquid physics [10–12, 14]. Here we explore the crossover between a SC Luttinger liquid and the SI regime in a pseudo-spin-1/2 gas of ^{6}Li atoms loaded into an array of 1D waveguides. We use Bragg spectroscopy to show the suppression of spin-charge separation and the systematic loss of coherence with increasing T. Surprisingly, signatures of the spin degree of freedom persist even for $T > T_F$, where T_F is the Fermi temperature.

Spin-charge separation arises from an energy gap between the excitation energies at fixed momentum $\hbar q$ for the spin and the charge sectors of the TLL Hamiltonian. We associate the energies of the spin- and charge-density waves by E_s and E_c, respectively. The speed of the SDW is less than that of the CDW[1], and thus $E_s < E_c$ in the SC regime. In the SI regime, where $k_BT > E_s$, the spin configurations are mixed, even while the charge correlations remain unaffected. Consequently, the CDW remains the dominant propagating mode [32]. For sufficiently high T, such that $k_BT > E_c$, the coherence in both sectors is expected to vanish, thus defining the charge-incoherent (CI) regime. The interplay between T, interaction strength, and waveguide occupancy N defines an energy hierarchy for the Luttinger liquid, as shown schematically in Fig. 1b. These regimes, whose properties are not well understood[27], are expected to be separated by smooth crossovers.

Our methods for preparing and probing quantum degenerate, pseudo-spin-1/2 Fermi gases of ^{6}Li atoms, and characterizing them by Bragg spectroscopy, have been described previously[12, 14, 39] (see Methods). We realize a pseudo-spin-1/2 system using a balanced spin mixture of the lowest and third-to-lowest hyperfine ground states of ^{6}Li, which we label as $|1\rangle$ and $|3\rangle$. The interactions depend on the s-wave scattering length, a, which is fixed to be 500 a_0, where a_0 is the Bohr radius, by using the $|1\rangle$-$|3\rangle$ magnetic Feshbach resonance located at 690 G [40]. We found that 500 a_0 is the largest value of a achievable without incurring an unacceptably large atom loss arising from 3-body recombination [12].

We vary T by modifying the duration and depth of the evaporative cooling trajectory first in a crossed-beam dipole trap and then in a 3D "dimple" trap. Following evaporation, the atoms are loaded into a 3D optical lattice, and then into a 2D optical lattice with a depth of 15 E_r, where $E_r = 1.4$ µK is the recoil energy due to a lattice photon of wavelength 1064 nm. The result is a sample of 6.5×10^4 atoms distributed over an array of quasi-1D tubes. The Gaussian curvature in our confining beams results in an inhomogeneous number profile, $N(r)$, where r is the cylindrical coordinate perpendicular to the axis of each waveguide. We compensate for this effect by introducing anti-confining, single-passed laser beams (532 nm) along each of the three orthogonal directions during the 3D lattice ramping[12, 39]. Adjusting the power of the anti-confining beams allows us to maintain a comparable $N(r)$ profile for each value of T within a range $\Delta T \lesssim 1$ µK. We focused our studies on the range of 500-1500 nK, which is found to cover the incoherent regimes, SI and CI, while still distinguishing a clear spin-charge separation ($v_s < v_c$) at the lower end of the range of T. Our lowest T of 500 nK is approximately twice the temperature used in Ref. 14. Because the highest T accessed is sufficiently below the radial confinement energy, the atoms are in the quasi-1D regime in all cases.

Bragg spectroscopy can be used to separately excite density waves in the charge (spin) sector by appropriately detuning the Bragg beams to generate a symmetric (antisymmetric) light shift with respect to the two spin states [14] (Supplementary Fig. 1). Since the Bragg pulse imparts both a momentum $\hbar q$ and an energy quantum $\hbar\omega$ per atom, we can determine the speed of propagation of the excitations (see Methods). The Bragg-induced momentum kick results in outcoupling a fraction of the atoms, the size of which constitutes the measurement signal[10, 12, 14]. It can be shown that this value is directly proportional to the dynamic structure factor $S_{s,c}(q, \omega)$ of the gas [41–43], which encodes the density-density correlations [44] in the spin and charge sectors, denoted by subscripts "s" and

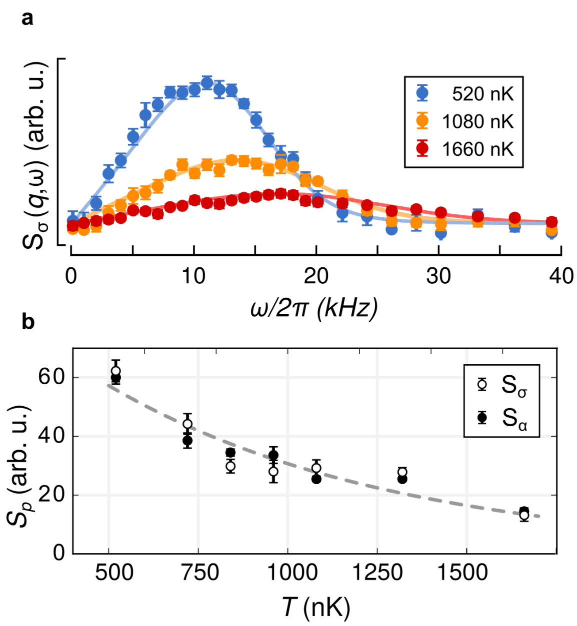

Fig. 2. Temperature effects on density waves. **a**, Bragg signal corresponding to $S_\sigma(q,\omega)$ for different temperatures. Each data-point is the average of at least 20 separate experimental shots. Solid lines are a fit to the Bragg spectra using a free-fermion theory with fit parameter T (see Methods). **b**, Peak amplitude S_p of the Bragg spectra as a function of T, where empty circles correspond to a symmetric Bragg excitation, S_σ, while filled circles represent the antisymmetric excitation, S_α. The dark-gray dashed line is a fit to T, assuming an exponential dependence, signaling the loss of correlations due to thermal fluctuations. Error bars represent standard error, obtained via bootstrapping (see Methods for details).

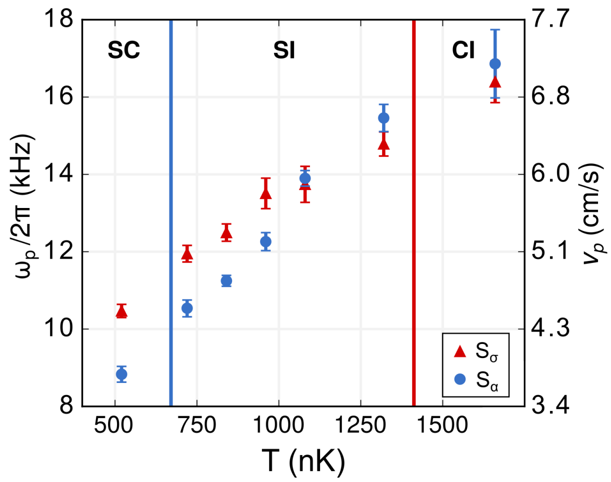

Fig. 3. Suppression of spin-charge separation. Frequencies at the peak amplitude of measured Bragg spectra for symmetric (red triangles) and antisymmetric (blue circles) excitations as a function of T. The corresponding speed of sound $v_p = \omega_p/q$ is given by the right axis. Error bars are the statistical standard errors of the extracted peak frequency obtained via a quadratic regression (see Methods). At sufficiently high T, only charge waves propagate, as the loss of spin coherence suppresses the separation of the collective density waves. Solid vertical lines correspond to the boundaries of the thermal hierarchy evaluated for $N = 30$ and $a_s = 500\ a_0$.

"c", respectively.

Representative Bragg spectra, corresponding to several values of T, are shown in Fig. 2a. We determine T for these by fitting the measured $S_c(q,\omega)$ to a free-fermion theory for which the density inhomogeneity is accounted for by the local density approximation, as in our previous work[12, 14]. We observe an overall suppression of the excitation amplitude with increasing T (Fig. 2b). This is indicative of the loss of coherence, and therefore, correlations. The measured peak amplitudes S_p are the same for both modes, within uncertainty, and they follow an exponential dependence on T, in agreement with a previous theoretical study of the role of temperature that predicted exponential decay of correlations with increasing T, as the system departs the SC regime[28]. While the CI regime has yet to be characterized, we associate the decay in the Bragg response to the loss of density-density correlations due to the proliferation of holes, suppressing the coherent propagation of either mode.

The atoms should respond only to a Bragg excitation with a symmetric light shift in the SI regime, since spin correlations are suppressed there[29, 32]. During the crossover between the SC and the SI regimes the Luttinger liquid will be averaged over an increasing number of spin configurations that have regions of local spin-imbalance (see Fig. 1a). Due to these regions, the Bragg pulse used to excite the spin-mode no longer has a locally antisymmetric response. Rather, with increasing T this Bragg pulse progressively couples to the charge-mode as the system crosses into the SI regime. We therefore label the measured signals as S_σ and S_α for symmetric and antisymmetric light shifts, instead of S_c and S_s, with corresponding propagation speeds v_σ and v_α. As T is increased, we observe a gradual suppression of the separation between v_σ and v_α (Fig 3), which is indicative of the increasing charge-mode character induced by the antisymmetric excitation pulse. The extent of this thermal disruption is affected both by the tube-to-tube occupancy variation and by the density inhomogeneity within each tube, as relatively low local density inevitably occurs near the confinement edges of the waveguide.

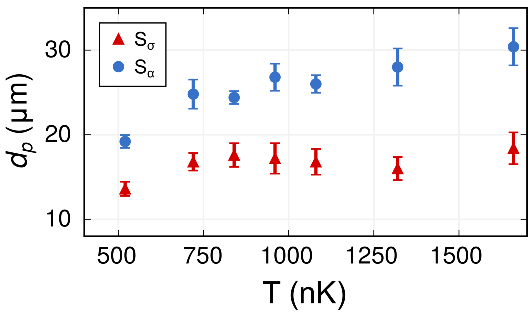

Fig. 4. Dispersion of incoherent density waves. $1/e^2$ axial width of out-coupled atoms, d_p, following a Bragg pulse and 150 μs time-of-flight expansion for symmetric (red triangles) and antisymmetric (blue circles) excitations as a function of T. The widths are the Gaussian fits to the positive outcoupled signal at ω_p[14]. Error bars are standard errors determined by bootstrapping for at least 20 independent images. The spin-density waves show an increased width arising from the reduced lifetime of the SDW excitation caused by back-scattering. The difference between the symmetric $S_\sigma(q,\omega)$ and antisymmetric $S_\alpha(q,\omega)$ excitations remains, even after the system is fully thermal.

The excitation energy for each sector is given by $E_{s,c} = \hbar n v_{s,c}$, where v_s and v_c are the propagation speeds of each mode, and n is the 1D density. We evaluate the propagation speeds for both modes by using the Bethe ansatz[45]. We extract the density at the center of each tube (and consequently the Fermi velocity v_F) from *in situ* phase-contrast images of the atom cloud [12, 14] (see Methods). An estimated upper bound for the crossover temperatures is found by evaluating the thermal hierarchy at the center of a single tube, located at $r = 0$, where the maximum occupancy is $N \simeq 30$. The resulting energy scales are $E_s \sim k_B \times 630$ nK and $E_c \sim k_B \times 1330$ nK, which are shown as solid lines in Fig. 3. For $T > 1000$ nK, we find that $v_\sigma \simeq v_\alpha$, to within our uncertainty, indicating a full suppression of spin-charge separation. Our measurements confirm that in the SI regime, the peak excitation frequency and the high-energy tails of $S(q,\omega)$ for each sector are identical to within their uncertainty (see Supplementary Fig. 2). To our knowledge this is the first experimental demonstration of thermal disruption of spin-charge separation.

We further characterized the Bragg spectra as a function of T by measuring the width of the outcoupled atoms d_p as a result of the Bragg perturbation after time-of-flight (Fig. 4). We have previously shown that d_p for the spin-mode increases with interaction strength, indicating non-linear effects in the spin-mode dispersion that are not present in charge excitations. We showed that the non-linearity is related to the finite lifetime of the SDW excitation due to back-scattering[14]. Remarkably, although both excitations propagate at the same speed for a sufficiently high temperature, we nonetheless observe a difference in d_p between the symmetric and antisymmetric excitations, even after the system has become fully thermal. Although mixing of the spin configurations suppresses spin-charge separation, we find, nonetheless, that the spin sector is not fully decoupled at these elevated temperatures, as Bragg spectroscopy still distinguishes features associated with the non-linear character of the spin sector. This is perhaps surprising given the expectation of universal spin physics in the SI regime, and suggests further study of the effects of nonlinearity on the decay of spin correlations is necessary[28].

In conclusion, we have characterized the temperature crossover between a coherent and an incoherent Luttinger liquid, as evidenced by the exponential decay of correlations as the system transitions into the SI regime. We observe a full suppression of spin-charge separation—one of the hallmarks of the standard TLL theory—clearly demonstrating the signatures of a disrupted Luttinger liquid. Further work using spin-sensitive imaging can focus on the measurement of density-density correlations functions, as well as exploring the anomalous exponents in the decay of charge and spin correlations. Our measurements can also be readily extended to a systematic study of more exotic regimes of 1D fermions. A gas with attractive interactions ($a < 0$) is predicted to realize the Luther-Emery liquid phase[46], which exhibits a gap only in the spin sector and is a potential 1D analog of a superconductor[47]. Another interesting path of study would be the characterization of a spin-imbalanced sample, where a quantum-critical region is expected to appear at finite temperatures for repulsive interactions[22], and new emergent liquid and gas-like quantum phases near a quantum phase transition could potentially be studied.

ACKNOWLEDGEMENTS

We thank G. Fiete, and H. Pu for helpful suggestions. This work was supported in part by the Army Research Office Multidisciplinary University Research Initiative (Grant No. W911NF-17-1- 0323) and the NSF (Grant No. PHY-2011829). D. C.-C. acknowledges financial support from CONACyT (Mexico, Scholarship No. 472271)

* randy@rice.edu

[1] F. D. M. Haldane, J. Phys. C **12**, 4791 (1979).
[2] A. Recati, P. O. Fedichev, W. Zwerger, and P. Zoller, Phys. Rev. Lett. **90**, 020401 (2003).
[3] C. Kollath, U. Schollwöck, and W. Zwerger, Phys. Rev. Lett. **95**, 176401 (2005).
[4] J. Y. Lee, X.-W. Guan, K. Sakai, and M. Batchelor, Phys. Rev. B **85**, 085414 (2012).
[5] X.-W. Guan, M. T. Batchelor, and C. Lee, Rev. Mod. Phys. **85**, 1633 (2013).
[6] M. Mestyán, B. Bertini, L. Piroli, and P. Calabrese, Phys. Rev. B **99**, 014305 (2019).
[7] T. Kinoshita, T. Wenger, and D. S. Weiss, Science **305**, 1125 (2004).
[8] T. Kinoshita, T. Wenger, and D. S. Weiss, Nature **440**, 900 (2006).
[9] Y.-a. Liao, A. S. C. Rittner, T. Paprotta, W. Li, G. B. Partridge, R. G. Hulet, S. K. Baur, and E. J. Mueller, Nature **467**, 567 (2010).
[10] G. Pagano, M. Mancini, G. Cappellini, P. Lombardi, F. Schäfer, H. Hu, X.-J. Liu, J. Catani, C. Sias, M. Inguscio, and L. Fallani, Nat. Phys. **10**, 198 (2014).
[11] B. Yang, Y.-Y. Chen, Y.-G. Zheng, H. Sun, H.-N. Dai, X.-W. Guan, Z.-S. Yuan, and J.-W. Pan, Phys. Rev. Lett. **119**, 165701 (2017).
[12] T. L. Yang, P. Grišins, Y. T. Chang, Z. H. Zhao, C. Y. Shih, T. Giamarchi, and R. G. Hulet, Phys. Rev. Lett. **121**, 103001 (2018).
[13] J. Vijayan, P. Sompet, G. Salomon, J. Koepsell, S. Hirthe, A. Bohrdt, F. Grusdt, I. Bloch, and C. Gross, Science **367**, 186 (2020).
[14] Senaratne, R. and Cavazos-Cavazos D., et al. Science **376**, 1305–1308 (2022).
[15] S.-I. Tomonaga, Prog. Theor. Phys. **5**, 544 (1950).
[16] J. M. Luttinger, J. of Math. Phys. **4**, 1154 (1963).
[17] F. D. M. Haldane, J. Phys. C **14**, 2585 (1981).
[18] J. Voit, J. of Phys.: Cond. Matt. **5**, 8305 (1993).
[19] T. Giamarchi, *Quantum Physics in One Dimension* (Oxford University Press, Oxford, 2003).
[20] A. J. Schofield, Contemp. Phys. **40**, 95 (1999).
[21] A. Imambekov, T. L. Schmidt, and L. I. Glazman, Rev. Mod. Phys. **84**, 1253 (2012).
[22] F. He, Y.-Z. Jiang, H.-Q. Lin, R. G. Hulet, H. Pu, and X.-W. Guan, Phys. Rev. Lett. **125**, 190401 (2020).
[23] A. Imambekov and L. I. Glazman, Science **323**, 228 (2009).
[24] A. Vishwanath and D. Carpentier, Phys. Rev. Lett. **86**, 676 (2001).
[25] S. Biswas, T. Mishra, S. Rao, and A. Kundu, Phys. Rev. B **102**, 155428 (2020).
[26] A. M. Chang, Rev. Mod. Phys. **75**, 1449 (2003).
[27] G. A. Fiete, Rev. Mod. Phys. **79**, 801 (2007).
[28] V. V. Cheianov and M. B. Zvonarev, Phys. Rev. Lett. **92**, 176401 (2004).
[29] K. A. Matveev, Phys. Rev. Lett. **92**, 106801 (2004); Phys. Rev. B **70**, 245319 (2004).
[30] G. A. Fiete and L. Balents, Phys. Rev. Lett. **93**, 226401 (2004).
[31] A. E. Feiguin and G. A. Fiete, Phys. Rev. B **81**, 075108 (2010).
[32] P. Kakashvili and H. Johannesson, Phys. Rev. B **76**, 085128 (2007).
[33] P. Kakashvili, S. G. Bhongale, H. Pu, and C. J. Bolech, Phys. Rev. A **78**, 041602 (2008).
[34] H. H. Jen and S.-K. Yip, Phys. Rev. A **95**, 053631 (2017).
[35] J. Decamp, J. Jünemann, M. Albert, M. Rizzi, A. Minguzzi, and P. Vignolo, Phys. Rev. A **94**, 053614 (2016).
[36] O. M. Auslaender, H. Steinberg, A. Yacoby, Y. Tserkovnyak, B. I. Halperin, K. W. Baldwin, L. N. Pfeiffer, and K. W. West, Science **308**, 88 (2005).
[37] H. Steinberg, O. Auslaender, A. Yacoby, J. Qian, G. A. Fiete, Y. Tserkovnyak, B. Halperin, K. Baldwin, L. N. Pfeiffer, and K. W. West, Phys. Rev. B **73**, 113307 (2006).
[38] G. A. Fiete, K. Le Hur, and L. Balents, Phys. Rev. B **72**, 125416 (2005).
[39] R. A. Hart, P. M. Duarte, T.-L. Yang, X. Liu, T. Paiva, E. Khatami, R. T. Scalettar, N. Trivedi, D. A. Huse, and R. G. Hulet, Nature **519**, 211 (2015).
[40] G. Zürn, T. Lompe, A. N. Wenz, S. Jochim, P. S. Julienne, and J. M. Hutson, Phys. Rev. Lett. **110**, 135301 (2013).
[41] J. Stenger, S. Inouye, A. P. Chikkatur, D. M. Stamper-Kurn, D. E. Pritchard, and W. Ketterle, Phys. Rev. Lett. **82**, 4569 (1999).
[42] A. Brunello, F. Dalfovo, L. Pitaevskii, S. Stringari, and F. Zambelli, Phys. Rev. A **64**, 063614 (2001).
[43] S. Hoinka, M. Lingham, M. Delehaye, and C. J. Vale, Phys. Rev. Lett. **109**, 050403 (2012).
[44] D. Pines, *Theory of quantum liquids: normal Fermi Liquids* (CRC Press, 2018).
[45] M. T. Batchelor, M. Bortz, X.-W. Guan, and N. Oelkers, in *Journal of Physics: Conference Series*, Vol. 42 (IOP Publishing, 2006) p. 002.
[46] A. Luther and V. J. Emery, Phys. Rev. Lett. **33**, 589 (1974).
[47] A. Seidel and D.-H. Lee, Phys. Rev. B **71**, 045113 (2005).
[48] M. Olshanii, Phys. Rev. Lett. **81**, 938 (1998).

METHODS

Temperature control for different samples. The final temperature T is determined by the evaporative cooling trajectory realized in a 1070 nm crossed-beam dipole trap, followed by further evaporation in a 3D harmonic trap produced by the intersection of three mutually-orthogonal focused trapping beams of wavelength 1064 nm. We vary the duration and final evaporation depth at each stage to control T while maintaining an approximately constant total atom number. The temperature has a significant effect on the tube-to-tube number distribution $N(r)$. The central tube occupancy is highest for low T and it diminishes with increasing T. We partially compensate these variations by introducing repulsive (532 nm) compensation laser beams along the three lattice directions, which are ramped on during the turn-on of the 3D optical lattice[39]. This enables us to adjust the degree of confinement in the optical lattice so that $N(r)$ is made approximately independent of T. The spin-charge separation we report in Fig. 3 for the lowest T is smaller in magnitude than in our previous report [14]. This difference is a consequence of the lowest T being 500 nK in the present experiment, while $T = 250$ nK for the experiment reported in Ref. 14.

Two-photon Bragg spectroscopy. This method allows us to independently address the density waves in the spin and the charge sectors by choosing the relative detuning between the spin states and an excited state (see Supplementary Fig. 1). As $T \to 0$, a symmetric light shift with respect to both spin states excites only CDWs while an antisymmetric one only excites SDWs. The experimental conditions for probing and analysing the resulting low-energy excitation spectra are the same as those previously reported in Ref. 14. The Bragg pulse duration is 200 μs and the atoms are imaged after 150 μs of time-of-flight. We adjust the angle between the Bragg beams such that for both modes the Bragg wave-vector is parallel to the tube axis and has a magnitude $|\vec{q}| = 1.47\ \mu\text{m}^{-1}$, corresponding to 0.3 k_F for the central tube. We calculate the Bragg signal by quantifying the number of atoms that receive a momentum kick from the Bragg pulse as a function of ω. This Bragg signal is proportional to the dynamic structure factor $S(q, \omega)$ [10, 12, 14, 42, 43].

Crossover hierarchy evaluation. The energy scales for the charge and spin sectors can be approximated as $E_\eta = \hbar n v_\eta$ (Ref. 27), where n is the 1D density, v_η is the propagation velocity of each mode, and $\eta =$ s,c correspond to either charge or spin sectors, respectively. We express E_η as $E_\eta(a, N)$, with a being the s-wave scattering length and N the tube occupancy. The density $n(a, N)$ is calculated by using the local density approximation (LDA) [12, 14], where we numerically solve the equation:

$$\mu - \frac{1}{2} m\omega_z^2 x^2 = \frac{\hbar^2\pi^2}{8m}\left[n(x)\right]^2 + \frac{g(a)}{2}[n(x)],$$

where μ is the chemical potential defined by $N = \int n(x)dx$, m is the atomic mass, ω_z is the axial angular trapping frequency, and $g(a) = \frac{2\hbar^2}{m}\left(\frac{a}{a_\perp^2}\right)\frac{1}{1-C(a/a_\perp)}$ is the interaction strength[48], where $C = |\xi(1/2)|/\sqrt{2} \sim 1.03$ and $a_\perp = \sqrt{\hbar/m\omega_\perp}$ is the length scale of the transverse harmonic confinement for a radial angular trapping frequency $\omega_\perp$. The propagation velocity for each mode $v_{s,c}$ can be expressed as $v_\eta = v_F \beta_\eta$, where v_F is the Fermi velocity, explicitly given by $v_F = \sqrt{\frac{\hbar}{m} N\omega_z}$. The factor β_η can be calculated exactly from the zero-temperature Bethe ansatz[45], although a first order approximation can be given as

$$\beta_\eta \simeq \sqrt{1 \pm \frac{2\gamma}{\pi^2}},$$

where the "+" sign corresponds to charge and the "−" sign to spin, and γ is the Lieb-Liniger parameter:

$$\gamma(a, n(a, N)) = \frac{a}{a_\perp^2 n}\frac{1}{1 - C\,(a/a_\perp)}.$$

Thus, we can express the energy scales as:

$$E_\eta(a, N) \simeq \hbar n(a, N) v_F(N)\sqrt{1 \pm \frac{2\gamma(a, n(a, N))}{\pi^2}}.$$

For Fig. 1 we evaluated the density at the center of a waveguide characterized by $\omega_\perp = 2\pi \times 227$ kHz and $\omega_z = 2\pi \times 1.3$ kHz, which corresponds to the quasi-1D geometry created by a 2D optical lattice with a depth of 15 E_r. The energy hierarchy defines the spin-coherent (SC), spin-incoherent (SI) and charge-incoherent (CI) regimes:

$$\begin{array}{ll} \textbf{SC} & k_B T < E_s < E_c \\ \textbf{SI} & E_s < k_B T < E_c \\ \textbf{CI} & E_s < E_c < k_B T. \end{array}$$

We evaluate the boundaries for the SC-SI and SI-CI regimes, shown with dashed lines in Fig. 1b, by the conditions $E_s = k_B T$ and $E_c = k_B T$, respectively. For our parameters, $E_s \sim k_B \times 630$ nK and $E_c \sim k_B \times$ 1330 nK.

SUPPLEMENTARY MATERIALS

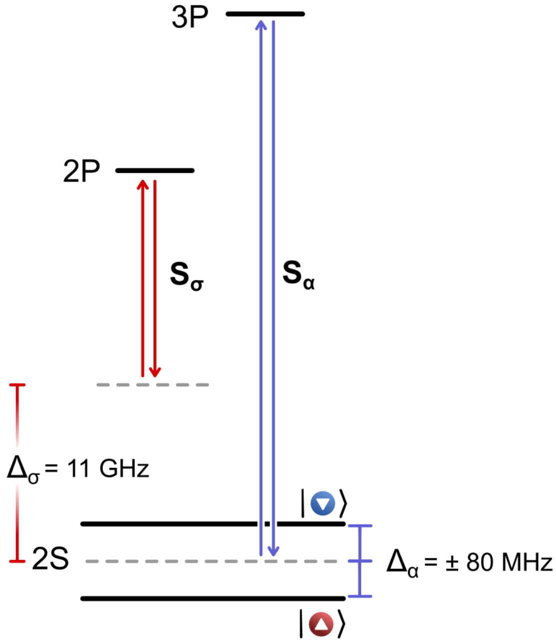

Supplementary Fig. 1. Symmetric and antisymmetric excitations via Bragg spectroscopy. Partial energy-level diagram of ^{6}Li showing relevant transitions and laser detunings of the Bragg pulses. We generate a symmetric light shift by symmetrically detuning the frequency of the Bragg beams far ($\Delta_\sigma = 11$ GHz) from the $2S \to 2P$ resonance. For an antisymmetric excitation, the Bragg beams are detuned by $\Delta_\alpha = \pm 80$ MHz from the $2S \to 3P$ resonance frequency.

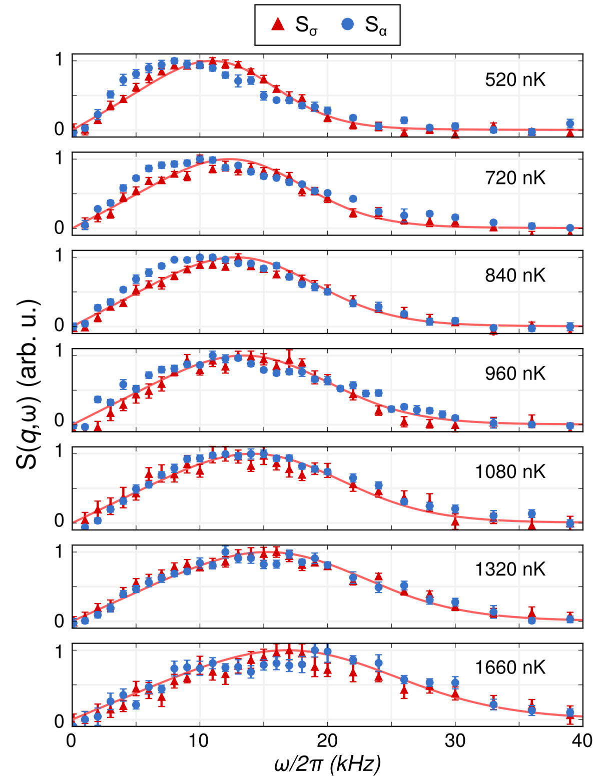

Supplementary Fig. 2. Bragg spectra. Normalized Bragg signals related to $S_\sigma(q,\omega)$ (red triangles) and $S_\alpha(q,\omega)$ (blue circles) excitations as a function of T. Each data-point is the average of at least 20 separate experimental shots. Solid lines are a fit to the Bragg spectra using a free-fermion theory with fit parameter T, which is labeled on the upper right corner for each case (see Methods). As T is increased, $S_\sigma(q,\omega)$ and $S_\alpha(q,\omega)$ become identical to within uncertainties. Error bars represent standard error, obtained via bootstrapping.